Spectral characterization of V-type asteroids – I. Space weathering effects and implications for V-type NEAs

Daniele Fulvio, Davide Perna, Simone Ieva, Rosario Brunetto, Zuzana Kanuchova, Carlo Blanco, Giovanni Strazzulla, Elisabetta Dotto

Monthly Notices
of the
ROYAL ASTRONOMICAL SOCIETY

MNRAS **455,** 584–595 (2016) doi:10.1093/mnras/stv2300

Spectral characterization of V-type asteroids – I. Space weathering effects and implications for V-type NEAs

Daniele Fulvio,[1⋆] Davide Perna,[2] Simone Ieva,[3] Rosario Brunetto,[4] Zuzana Kanuchova,[5] Carlo Blanco,[6,7] Giovanni Strazzulla[6] and Elisabetta Dotto[3]

[1]*Departamento de Física, Pontifícia Universidade Católica do Rio de Janeiro, Rua Marquês de São Vicente 225, 22451-900 Rio de Janeiro, RJ, Brazil*
[2]*LESIA, Observatoire de Paris, PSL Research University, CNRS, Sorbonne Universités, UPMC Univ. Paris 06, Univ. Paris Diderot, Sorbonne Paris Cité, 5 place Jules Janssen, F-92195 Meudon, France*
[3]*INAF – Osservatorio Astronomico di Roma, Via Frascati 33, I-00040 Monte Porzio Catone, Roma, Italy*
[4]*Institut d'Astrophysique Spatiale, CNRS, UMR-8617, Université Paris-Sud, bâtiment 121, F-91405 Orsay Cedex, France*
[5]*Astronomical Institute of the Slovak Academy of Sciences, 059 60 Tatranská Lomnica, Slovakia*
[6]*INAF – Osservatorio Astrofisico di Catania, Via S. Sofia 78, I-95123 Catania, Italy*
[7]*Dipartimento di Fisica e Astronomia, Università di Catania, Via S. Sofia 78, I-95123 Catania, Italy*

Accepted 2015 October 1. Received 2015 October 1; in original form 2015 August 19

ABSTRACT

Among main belt asteroids, V-types belonging to Vesta's dynamical family are known as 'Vestoids' while those lying outside Vesta's family as 'non-Vestoids'. V-types have also been found within the population of Near Earth Asteroids (NEAs). Several questions on Vesta, the V-types, and the Howardite–Eucrite–Diogenite meteorites are still unsolved, such as the genesis of each class/subclass, their evolution and mutual relationship, and the existence of other basaltic parent bodies. We present new NIR (0.8–2.4 μm) spectroscopic observations of seven non-Vestoids, carried out at the Telescopio Nazionale Galileo (TNG – INAF). We derived a number of spectral parameters (BI and BII centres, band separations, and BI slopes) and compared them with available spectra of V-types belonging to different subclasses (102 V-types in total), to highlight possible spectral differences useful to shed light on the questions mentioned above. We also considered the data from ion irradiation experiments performed on different samples of eucrites, simulating space weathering effects. Net discrepancies are seen for the BI slope distributions: NEAs show a distribution strongly different from all other V-type subclasses. Ion irradiation experiments induce strong effects on BI slope values and, as irradiation proceeds, the BI slope of eucrites quickly increases, changing the overall aspect of their VIS–NIR spectra (0.4–2.5 μm). Space weathering may explain the whole range of spectral slopes observed for all V-type subclasses. An exception is represented by NEAs, where moderate space weathering effects are evidenced. We propose that this is due to tidal perturbations exposing 'fresh' unweathered surface grains during close encounters with the Earth, as previously found for Q-type NEAs.

Key words: methods: laboratory: atomic – techniques: spectroscopic – meteorites, meteors, meteoroids – minor planets, asteroids: individual: Vesta – infrared: general.

1 INTRODUCTION

Asteroid (4) Vesta is the largest differentiated main belt object showing a basaltic crust. The basaltic composition of its surface has been discovered by McCord, Adams & Johnson (1970), later on confirmed by many observations (e.g. McFadden, McCord & Pieters 1977; Binzel et al. 1997; Gaffey 1997; Vernazza et al. 2005) and strengthen by the extensive and detailed data provided by the Dawn spacecraft's visible and infrared spectrometer VIR (De Sanctis et al. 2012). The Dawn spacecraft data show that the 1 and 2 μm pyroxene signatures (hereafter BI and BII, respectively) are present ubiquitously across Vesta surface and confirm that Vesta surface composition is similar to that of the Howardite–Eucrite–Diogenite meteorites (HEDs). Nevertheless, HEDs lithologies are present on Vesta with spectral variations at both large and small scale across its surface and, overall, Vesta mineralogy indicates a complex geological and collisional history (De Sanctis et al. 2012; Jaumann et al. 2012; Russell et al. 2012).

In recent years, several tens of asteroids have been found to show a surface composition similar to that of Vesta and have been classified as 'V-types'. Many of these objects belong to the Vesta's

⋆ E-mail: dfulvio@puc-rio.br; dfu@oact.inaf.it

Table 1. Orbital parameters, absolute magnitude, diameter, and dynamical subclass of the observed asteroids.

Object	a (au)	e	i (°)	H	Diameter (km)	Dynamical subclass
(1914) Hartbeespoortdam	2.406	0.148	5.678	12.0	8.4	Low-i
(1946) Walraven	2.293	0.236	8.166	12.0	8.4	Fugitives
(2486) Metsähovi	2.269	0.080	8.410	12.4	7.0	Fugitives
(2566) Kirghizia	2.450	0.079	5.081	12.3	7.3	Low-i
(2912) Lapalma	2.289	0.071	7.276	12.4	7.0	Fugitives
(3153) Lincoln	2.423	0.130	7.707	12.7	6.1	IOs
(3869) Norton	2.453	0.126	4.362	13.0	5.3	Low-i

dynamical family ('Vestoids') and are believed to derive from the huge collisional event responsible for the large craters near the south pole of Vesta (Thomas et al. 1997; Marchi et al. 2012). The discovery of V-types outside the limits of Vesta's dynamical family (Zappala et al. 1995; Migliorini et al. 1997; Carruba et al. 2005) called this picture into question and, although, dynamical simulations showed that some 'non-Vestoids' could be fugitives from the Vesta family (Nesvorný et al. 2008; Roig et al. 2008), many other non-Vestoids do not show any clear dynamical link to Vesta, suggesting, thus, that they could be fragments of distinct differentiated parent bodies (Lazzaro et al. 2000; Duffard et al. 2004; Alvarez-Candal et al. 2006). The existence of other basaltic parent bodies seems to be also supported by recent studies on the HEDs. As mentioned before, reflectance spectra of Vesta and V-type asteroids are similar to those of the HEDs. This unique agreement was considered the main evidence that Vesta is the parent body of the HEDs, although Vesta itself was not believed to be their direct source. The more realistic scenario foresaw a link between Vesta and the HEDs via basaltic fragments that reached the Earth through complex dynamical processes (see Binzel et al. 2004 and references therein). However, recent measurements on oxygen isotopic composition of HEDs have indicated that, although most of them come from the same basaltic parent body, few others do not match this view (see for instance Scott et al. 2009).

In this study, we present new NIR (0.8–2.4 μm) spectra for seven non-Vestoids obtained at the Telescopio Nazionale Galileo (TNG-INAF, La Palma, Spain). We analysed and compared the NIR spectral properties of these asteroids and other available V-types belonging to different classes and subclasses, to highlight possible spectral differences that can help to shed light on the origin and evolution of V-types. Previous works (Duffard et al. 2004; Moskovitz et al. 2010; De Sanctis et al. 2011a,b) did not find any strong difference between Vesta, Vestoids, and non-Vestoids. However, we include in our spectral analysis, for the first time to the best of our knowledge, V-types belonging to the population of Near Earth Asteroids (NEAs) and a number of VIS-NIR (0.4–2.5 μm) data from ion irradiation experiments performed on HED meteorites to simulate the effects of space weathering processes on V-type asteroids' surface (Fulvio et al. 2012). We analyse and characterize our data set using band analysis techniques (e.g. Cloutis & Gaffey 1991; Gaffey et al. 2002) looking for statistically significant differences among the spectral properties of V-type asteroids belonging to different dynamical subclasses. A companion paper will be focusing on the mineralogical analysis of V-types (Ieva et al. 2015).

2 V-TYPES: DYNAMICAL SUBCLASSES

In order to highlight spectral differences and similarities among V-types, we first need a clear definition for their dynamical classes and subclasses. In this work, we consider as *vestoid* any V-type asteroid belonging to the Vesta dynamical family, as defined by Nesvorný (2012)[1] using the Hierarchical Clustering Method (HCM). V-types outside the limit of the Vesta dynamical family are collectively known as *non-Vestoid*. Among them, some objects could actually be fugitive members that escaped the family via the combined influence of mean motion and secular resonances and Yarkovsky effect (Nesvorný et al. 2008). Following the definition of Nesvorný et al. (2008), we consider *fugitive* any basaltic asteroid with semimajor axis <2.3 au and comparable e and i with the Vesta family. Among the remaining non-Vestoids, we consider two subclasses which deserve a special attention: (i) the *low-i* subclass, inner main belt V-types with low inclination ($i < 6°$ and $2.3 < a < 2.5$ au) that cannot be reconducted to a dynamical origin from Nesvorný et al. (2008) and (ii) the *MOVs* subclass: middle and outer main belt V-types which should have crossed the 3:1 resonance with Jupiter to have an origin compatible with Vesta. This last hypothesis is highly unlikely (Roig et al. 2008). Non-Vestoids in the inner main belt not belonging to any of the previously defined subclasses (fugitives, low-i, and MOVs) are here defined as *Inner Others* (IOs). Finally, *V-type NEA* is any V-type asteroid with perihelion $q < 1.3$ au. In this work, we consider a total of 102 V-types: 33 vestoids, 17 fugitives, 18 low-i, 11 IOs, 2 MOVs, and 21 NEAs.

3 OBSERVATIONS AND DATA REDUCTION

We observed seven non-Vestoids with missing NIR spectra (at the time of the observations; in the meanwhile an NIR spectrum of (2912) Lapalma has been published in De Sanctis et al. 2011a). Orbital parameters and absolute magnitude H of the targets are given in Table 1 (values are taken from the Minor Planet Center website[2]), together with their estimated diameters assuming an albedo of 0.4 (a characteristic value for basaltic asteroids) and the non-Vestoids dynamical subclass to which they belong to.

Spectroscopic observations were carried out at the 3.6 m TNG-INAF (La Palma, Spain). The observational circumstances are given in Table 2. We used the Near Infrared Camera Spectrometer (NICS), a multimode instrument based on a 1024 × 1024 pixel HgCdTe Hawaii array, equipped with an Amici prism disperser, which covers the 0.8–2.4 μm range with a varying spectral dispersion of 30–100 Å pixel^{-1} (http://www.tng.iac.es). Spectra were taken through a 2 arcsec wide slit oriented along the parallactic angle to avoid flux loss due to the differential refraction. The objects were nodded along the spatial direction of the slit, in order to obtain alternating pairs (A and B) of near-simultaneous images for the background removal, using exposure times of 90–120 s for each nodded spectrum (in few cases we used 140 s). Flat-fields and several spectra of solar analogue stars were also recorded during the observations.

[1] http://sbn.psi.edu/pds/resource/nesvornyfam.html
[2] http://minorplanetcenter.net/

Table 2. Observational circumstances of the observed asteroids.

Object	Date	UT_{start}	T_{exp} (s)	Air mass	Solar analogue (air mass)
(1914) Hartbeespoortdam	2009 Nov 09	05:52	8×120	1.60	Land. 98-978 (1.26)
	2009 Nov 10	02:57	4×120	1.04	Hyades 142 (1.05)
(1946) Walraven	2009 Apr 05	21:12	10×120	1.32	Land. 98-978 (1.26)
(2486) Metsähovi	2009 Nov 09	00:29	$8 \times 90 + 4 \times 120$	1.06	Land. 112-1333 (1.21)
(2566) Kirghizia	2009 Apr 05	22:42	10×120	1.39	Land. 98-978 (1.52)
(2912) Lapalma	2009 Nov 08	20:47	$4 \times 140 + 12 \times 120$	1.56	Land. 112-1333 (1.21)
	2009 Nov 09	20:57	12×120	1.56	Land. 112-1333 (1.23)
	2009 Nov 09	22:00	12×120	1.84	Land. 93-101 (1.38)
(3153) Lincoln	2009 Apr 06	01:26	10×120	1.15	Land. 107-998 (1.29)
(3869) Norton	2009 Nov 10	00:34	$8 \times 90 + 4 \times 120$	1.05	Hyades 142 (1.05)

The data were reduced with the software package MIDAS, using standard procedures (e.g. Perna et al. 2010; Ieva et al. 2014): flat-fielding, correction for spatial and spectral axes distortion, A-B (or B-A) subtraction for each pair of frames, shifting and adding of the frames, collapsing the two-dimensional spectra into one dimension. Wavelength calibration was first obtained using the look-up table available on the TNG website, which is based on the theoretical dispersion predicted by ray-tracing, and then refined to best fit the observed telluric bands. The reflectivity of each target was then obtained by dividing its spectrum by that of a solar analogue star observed just before or after the object, at air mass as similar as possible. The spectra were finally smoothed with a median filter technique (with a box of ∼5–10 pixel in the spectral direction and a threshold around 10 per cent). The resulting spectra are shown in Fig. 1, after combining them with visible data from Alvarez-Candal et al. (2006, for asteroids 1914, 1946, and 2486) and from the Small Main-Belt Asteroid Spectroscopic Survey[3] (for asteroids 2566, 2912, 3153, and 3869). Spectral extension towards the visible has been done for a proper evaluation of BI slopes (see Section 4). As clearly seen in Fig. 1, all spectra of the observed asteroids show the typical absorption bands near 1 and 2 μm (BI and BII, respectively) indicative of the presence of pyroxene and olivine and typical of V-type asteroids.

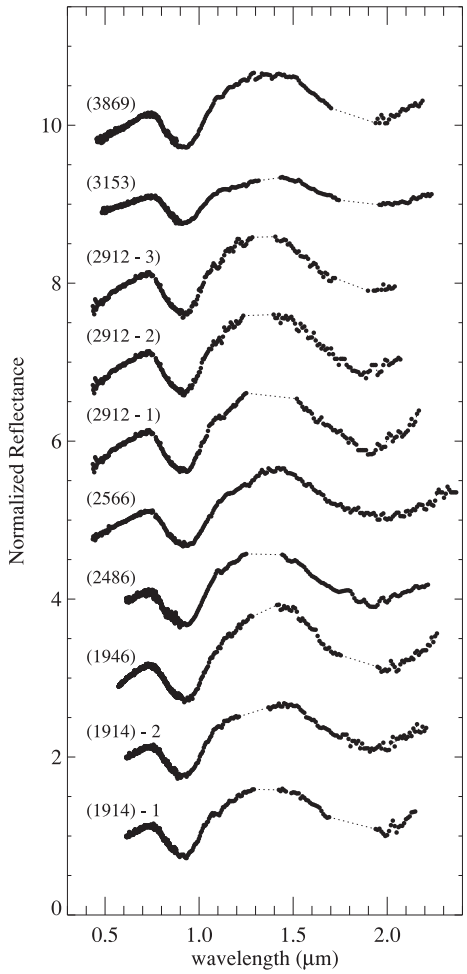

Figure 1. NIR spectra obtained at the TNG, shifted by 1.0 in reflectance for clarity. Spectral regions affected by strong atmospheric absorption (dashed lines) or low instrumental efficiency (typically longwards of ∼2.2 μm) have been cut out. Spectral extension below 0.8 μm has been done using data from the literature (see the text for details). All spectra are normalized to unity at 0.62 μm.

4 SPECTRAL ANALYSIS: STATISTICS AND DISTRIBUTIONS

Band analysis techniques are commonly used for analysing asteroids and meteorites spectral data. The relationship between spectral parameters and surface mineralogy of asteroids has been addressed in various papers over the last years (e.g. Gaffey et al. 2002; Klima, Pieters & Dyar 2007; De Sanctis et al. 2011a,b). In this paper, we do not focus on mineralogy properties as this will be one of the focus of a companion paper (Ieva et al., 2015). We rather use the results of band analysis techniques to look for statistically significant differences among the spectral properties of V-type asteroids belonging to different dynamical subclasses. We have considered the following parameters: minimum and central wavelength of BI and BII, Band separation, and BI slope. Unless otherwise specified, values of BI and BII minima are from the companion paper of Ieva et al. (2015). Band minima have been evaluated using standard procedures, fitting each band with a second-order polynomial fit. Band centres (μm) have been evaluated using the same procedure described in De Sanctis et al. (2011b). In particular, we want to make explicit that the relationships, (a) BI centre = BI minimum + 0.007 and (b) BII centre = BII minimum, have been used to derive band centres from band minima; Band separation (μm) is defined as the difference between BII and BI minima. Finally, BI slope (μm^{-1}) is defined as the spectral slope of the linear continuum across the BI band, from ∽0.7 μm to ∽1.4 μm. The slope of the BI band

[3] http://smass.mit.edu/smass.html

Table 3. Spectral parameters of V-types asteroids. We point out that typical BI slope errors are $\leq 0.02\ \mu m^{-1}$. When multiple observations of the same asteroid are considered, the average BI slope and error is reported.

Object	BI minimum (μm)	BII minimum (μm)	Band separation (μm)	BI centre (μm)	BI slope (μm^{-1})	Subclass
809 Lundia	0.921 ± 0.002	1.939 ± 0.001	1.02 ± 0.01	0.928 ± 0.002	1.05 ± 0.04	Fugitives
854 Frostia	0.950 ± 0.001	2.000 ± 0.002	1.05 ± 0.01	0.957 ± 0.001	0.21 ± 0.015	IOs
956 Elisa	0.922 ± 0.002	1.929 ± 0.002	1.01 ± 0.01	0.929 ± 0.002	0.91 ± 0.05	Fugitives
1459 Magnya	0.928 ± 0.001	1.923 ± 0.001	1.00 ± 0.01	0.935 ± 0.001	0.77 ± 0.03	MOVs
1468 Zomba	0.923 ± 0.002	1.973 ± 0.003	1.05 ± 0.01	0.930 ± 0.002	–	IOs
1914 Hartbeespoortdam[a]	0.909 ± 0.005	1.906 ± 0.01	0.997 ± 0.012	0.916 ± 0.005	0.87 ± 0.015	Low-i
1929 Kollaa	0.927 ± 0.003	1.957 ± 0.003	1.03 ± 0.01	0.934 ± 0.003	0.77 ± 0.2	Vestoids
1933 Tinchen	0.916 ± 0.008	1.939 ± 0.002	1.02 ± 0.01	0.923 ± 0.008	0.68 ± 0.2	Vestoids
1946 Walraven[a]	0.917 ± 0.005	1.939 ± 0.008	1.02 ± 0.01	0.924 ± 0.005	1.12 ± 0.03	Fugitives
1981 Midas	0.930 ± 0.002	2.020 ± 0.011	1.09 ± 0.01	0.937 ± 0.002	0.3 ± 0.1	NEAs
2011 Veteraniya	0.916 ± 0.002	1.952 ± 0.006	1.04 ± 0.01	0.923 ± 0.002	0.97 ± 0.02	Vestoids
2045 Peking	0.926 ± 0.002	1.939 ± 0.002	1.01 ± 0.01	0.933 ± 0.002	0.77 ± 0.1	Vestoids
2371 Dimitrov	0.920 ± 0.002	1.972 ± 0.006	1.05 ± 0.01	0.927 ± 0.002	0.92 ± 0.06	Low-i
2442 Corbett	0.922 ± 0.001	1.935 ± 0.001	1.01 ± 0.01	0.929 ± 0.001	0.78 ± 0.02	Low-i
2468 Repin[b]	0.922 ± 0.004	1.930 ± 0.03	1.008 ± 0.034	0.929 ± 0.004	–	Vestoids
2486 Metsahovi[a]	0.915 ± 0.005	1.931 ± 0.006	1.02 ± 0.008	0.922 ± 0.005	0.86 ± 0.01	Fugitives
2511 Patterson	0.925 ± 0.002	1.955 ± 0.004	1.03 ± 0.01	0.932 ± 0.002	0.72 ± 0.07	Vestoids
2566 Kirghizia[a]	0.925 ± 0.002	1.958 ± 0.006	1.03 ± 0.01	0.932 ± 0.002	0.64 ± 0.1	Low-i
2579 Spartacus	0.935 ± 0.004	1.990 ± 0.012	1.06 ± 0.02	0.942 ± 0.004	0.34 ± 0.3	Fugitives
2653 Principia	0.925 ± 0.001	1.964 ± 0.007	1.04 ± 0.01	0.932 ± 0.001	0.55 ± 0.1	Low-i
2763 Jeans	0.930 ± 0.002	1.995 ± 0.003	1.07 ± 0.01	0.937 ± 0.002	0.56 ± 0.2	Low-i
2795 Lepage	0.928 ± 0.002	1.950 ± 0.003	1.02 ± 0.01	0.935 ± 0.002	0.58 ± 0.08	Fugitives
2823 van der Laan	0.925 ± 0.001	1.953 ± 0.005	1.03 ± 0.01	0.932 ± 0.001	–	Low-i
2851 Harbin	0.920 ± 0.001	1.907 ± 0.004	0.99 ± 0.01	0.927 ± 0.001	0.69 ± 0.08	IOs
2912 Lapalma	0.920 ± 0.001	1.927 ± 0.003	1.01 ± 0.01	0.927 ± 0.001	0.83 ± 0.08	Fugitives
3153 Lincoln[a]	0.924 ± 0.005	1.955 ± 0.01	1.03 ± 0.01	0.931 ± 0.005	0.39 ± 0.01	IOs
3155 Lee	0.910 ± 0.002	1.913 ± 0.007	1.00 ± 0.01	0.917 ± 0.002	0.95 ± 0.1	Vestoids
3268 De Sanctis[b]	0.910 ± 0.004	1.976 ± 0.02	1.066 ± 0.024	0.917 ± 0.004	0.85 ± 0.015	Vestoids
3498 Belton	0.917 ± 0.006	1.889 ± 0.021	0.97 ± 0.03	0.924 ± 0.006	–	Vestoids
3613 Kunlun	0.960 ± 0.004	1.943 ± 0.006	0.98 ± 0.01	0.967 ± 0.004	–	Vestoids
3657 Ermolova	0.921 ± 0.001	1.919 ± 0.003	1.00 ± 0.01	0.928 ± 0.001	0.76 ± 0.06	Vestoids
3703 Volkonskaya	0.915 ± 0.004	1.932 ± 0.007	1.02 ± 0.01	0.922 ± 0.004	–	Vestoids
3782 Celle	0.920 ± 0.002	1.942 ± 0.004	1.02 ± 0.01	0.927 ± 0.002	0.54 ± 0.03	Vestoids
3869 Norton[a]	0.915 ± 0.004	1.913 ± 0.007	0.998 ± 0.01	0.922 ± 0.004	0.91 ± 0.02	Low-i
3908 Nyx	0.923 ± 0.003	1.943 ± 0.004	1.02 ± 0.01	0.930 ± 0.003	0.48 ± 0.1	NEAs
3944 Halliday[b]	0.912 ± 0.002	1.943 ± 0.02	1.03 ± 0.022	0.919 ± 0.002	0.43 ± 0.01	Vestoids
3968 Koptelov	0.922 ± 0.009	1.905 ± 0.001	0.98 ± 0.01	0.929 ± 0.009	0.55 ± 0.013	Vestoids
4038 Kristina	0.910 ± 0.003	1.963 ± 0.011	1.053 ± 0.01	0.917 ± 0.003	0.81 ± 0.2	Vestoids
4055 Magellan	0.920 ± 0.001	1.925 ± 0.003	1.01 ± 0.01	0.927 ± 0.001	0.28 ± 0.08	NEAs
4147 Lennon[b]	0.919 ± 0.003	1.926 ± 0.005	1.007 ± 0.013	0.926 ± 0.003	0.45 ± 0.02	Vestoids
4215 Kamo	0.920 ± 0.002	1.945 ± 0.014	1.03 ± 0.02	0.927 ± 0.002	0.34 ± 0.1	Vestoids
4383 Suruga[c]	0.913 ± 0.005	1.910 ± 0.01	1.00 ± 0.01	0.920 ± 0.009	–	IOs
4796 Lewis	0.925 ± 0.002	1.951 ± 0.008	1.03 ± 0.01	0.932 ± 0.002	0.732[d]	Low-i
4815 Anders[b]	0.931 ± 0.005	1.960 ± 0.03	1.029 ± 0.035	0.938 ± 0.005	–	Vestoids
4993 Cossard[b]	0.921 ± 0.003	2.071 ± 0.02	1.151 ± 0.023	0.928 ± 0.003	–	Vestoids
5111 Jacliff	0.920 ± 0.002	1.940 ± 0.001	1.02 ± 0.01	0.927 ± 0.002	0.62 ± 0.07	Vestoids
5481 Kiuchi	0.919 ± 0.002	1.939 ± 0.008	1.02 ± 0.01	0.926 ± 0.002	0.93 ± 0.015	Vestoids
5498 Gustafsson	0.928 ± 0.001	1.967 ± 0.002	1.04 ± 0.01	0.935 ± 0.001	0.986[d]	Low-i
5560 Amytis[c]	0.905 ± 0.005	1.90 ± 0.01	0.99 ± 0.01	0.912 ± 0.009	–	Fugitives
5604 1992 FE	0.918 ± 0.002	1.953 ± 0.009	1.04 ± 0.01	0.925 ± 0.002	0.23 ± 0.03	NEAs
6331 1992 FZ1	0.901 ± 0.002	2.054 ± 0.002	1.15 ± 0.01	0.908 ± 0.002	–	Vestoids

is highly representative of space weathering effects (see Hiroi & Sasaki 2001; Strazzulla et al. 2005; Fulvio et al. 2012). Values of the mentioned spectral parameters are reported in Table 3.

In Fig. 2 (left-hand panel), we plot BI centre versus BII centre for all the V-types considered in this work (Table 3). Vesta family members (Vestoids) tend to regroup in the region 0.91 μm $\leq BI_{centre} \leq$ 0.94 μm and 1.88 μm $\leq BII_{centre} \leq$ 1.98 μm, although few asteroids spread out towards higher BII centre (asteroids 4993, 6331, and 10320) or lower BI centre (asteroid 8693). One asteroid (3613) shows the highest BI centre value, at odds with the other Vestoids. All the non-Vestoids subclasses show BI and BII centre values comparable to those above mentioned for the Vestoids, except in few cases: asteroids 2579, 6406, and 9147 (fugitives); asteroids 2763 and 97276 (low-i); and asteroid 854 among the IOs; on the contrary, a shift towards higher BI and BII centre values seems to be shown by NEA V-types with respect to the Vestoids.

Table 3 – *continued*

Object	BI minimum (μm)	BII minimum (μm)	Band separation (μm)	BI centre (μm)	BI slope (μm^{-1})	Subclass
6406 1992 MJ[b]	0.916 ± 0.003	1.990 ± 0.02	1.074 ± 0.023	0.923 ± 0.003	–	Fugitives
6563 Steinheim[c]	0.924 ± 0.006	1.910 ± 0.01	0.99 ± 0.01	0.93 ± 0.01	–	Fugitives
6611 1993 VW	0.930 ± 0.001	2.000 ± 0.002	1.07 ± 0.01	0.937 ± 0.001	0.19 ± 0.03	NEAs
6976 Kanatsu[c]	0.911 ± 0.003	1.930 ± 0.01	1.02 ± 0.01	0.918 ± 0.007	–	IOs
7148 Reinholdbien	0.928 ± 0.008	1.942 ± 0.021	1.01 ± 0.03	0.935 ± 0.008	1.02 ± 0.02	Fugitives
7800 Zhongkeyuan	0.921 ± 0.002	1.932 ± 0.019	1.01 ± 0.02	0.928 ± 0.002	0.902[d]	Low-i
7889 1994 LX	0.930 ± 0.003	1.937 ± 0.005	1.01 ± 0.01	0.937 ± 0.003	0.15 ± 0.02	NEAs
8693 Matsuki[b]	0.892 ± 0.005	1.923 ± 0.02	1.031 ± 0.025	0.899 ± 0.005	–	Vestoids
8761 Crane[c]	0.925 ± 0.005	1.95 ± 0.01	1.02 ± 0.01	0.932 ± 0.009	–	IOs
9147 Kourakuen[c]	0.908 ± 0.001	1.87 ± 0.01	0.98 ± 0.01	0.915 ± 0.005	–	Fugitives
9481 Menchu	0.931 ± 0.001	1.931 ± 0.008	1.00 ± 0.01	0.938 ± 0.001	0.296[d]	Low-i
9531 Jean Luc[c]	0.930 ± 0.001	1.94 ± 0.01	1.01 ± 0.01	0.937 ± 0.006	–	Fugitives
9553 Colas	0.922 ± 0.001	1.923 ± 0.003	1.00 ± 0.01	0.929 ± 0.001	0.803[d]	Low-i
10320 1990 TR1[b]	0.917 ± 0.005	2.021 ± 0.03	1.104 ± 0.035	0.924 ± 0.005	–	Vestoids
10349 1992 LN	0.905 ± 0.005	1.922 ± 0.016	1.02 ± 0.02	0.912 ± 0.005	–	Vestoids
10614 1997 UH1[c]	0.919 ± 0.003	1.95 ± 0.01	1.03 ± 0.01	0.926 ± 0.007	–	Vestoids
11699 1998 FL105	0.916 ± 0.002	1.938 ± 0.003	1.02 ± 0.01	0.923 ± 0.002	0.74 ± 0.02	Vestoids
11764 Benbaillaud[c]	0.920 ± 0.005	1.97 ± 0.01	1.05 ± 0.01	0.927 ± 0.009	–	Fugitives
16416 1987 SM3	0.923 ± 0.003	1.963 ± 0.013	1.04 ± 0.02	0.930 ± 0.003	0.887[d]	Fugitives
16651 1993 TS11	0.925 ± 0.005	1.910 ± 0.011	0.99 ± 0.02	0.932 ± 0.005	–	Vestoids
17064 1999 GX16[c]	0.919 ± 0.005	1.94 ± 0.01	1.02 ± 0.01	0.926 ± 0.009	–	Vestoids
21238 Panarea	0.910 ± 0.004	1.887 ± 0.009	0.98 ± 0.01	0.917 ± 0.004	0.81 ± 0.03	MOVs
26886 1994 TJ2	0.913 ± 0.001	1.906 ± 0.007	0.99 ± 0.01	0.920 ± 0.001	0.877[d]	Low-i
27343 Deannashea	0.917 ± 0.002	1.914 ± 0.004	1.00 ± 0.01	0.924 ± 0.002	1.021[d]	Low-i
31692 1999 JQ31[c]	0.920 ± 0.003	1.93 ± 0.01	1.01 ± 0.01	0.927 ± 0.007	–	Low-i
31953 2000 GZ125[c]	0.929 ± 0.005	1.92 ± 0.01	0.99 ± 0.01	0.936 ± 0.009	–	Fugitives
32940 1995 UW4[c]	0.926 ± 0.001	1.91 ± 0.01	0.98 ± 0.01	0.933 ± 0.005	–	Fugitives
33881 2000 JK66	0.929 ± 0.001	1.930 ± 0.004	1.00 ± 0.01	0.936 ± 0.001	1.105[d]	IOs
36412 2000 OP49	0.930 ± 0.003	1.961 ± 0.010	1.03 ± 0.01	0.937 ± 0.003	0.999[d]	Low-i
38070 Redwine	0.932 ± 0.002	1.958 ± 0.007	1.03 ± 0.01	0.939 ± 0.002	0.377[d]	IOs
42947 1999 TB98	0.924 ± 0.008	1.928 ± 0.009	1.00 ± 0.02	0.931 ± 0.008	–	Vestoids
50098 2000 AG98	0.925 ± 0.002	1.947 ± 0.004	1.02 ± 0.01	0.932 ± 0.002	–	Vestoids
52750 1998 KK17	0.925 ± 0.002	1.985 ± 0.006	1.06 ± 0.01	0.932 ± 0.002	–	NEAs
61235 2000 OT15[c]	0.932 ± 0.002	1.93 ± 0.02	0.99 ± 0.02	0.939 ± 0.006	–	IOs
64276 2001TW218[c]	0.925 ± 0.002	1.96 ± 0.01	1.04 ± 0.01	0.932 ± 0.006	–	IOs
66268 1999 JJ3	0.923 ± 0.010	1.920 ± 0.011	1.00 ± 0.02	0.930 ± 0.010	–	Vestoids
88188 2000 XH44	0.920 ± 0.002	1.975 ± 0.003	1.06 ± 0.01	0.927 ± 0.002	–	NEAs
97276 1999 XC143	0.934 ± 0.002	2.025 ± 0.008	1.09 ± 0.01	0.941 ± 0.002	0.37[d]	Low-i
137924 2000 BD19	0.937 ± 0.005	1.952 ± 0.010	1.02 ± 0.01	0.944 ± 0.005	–	NEAs
192563 1998 WZ6	0.920 ± 0.003	2.005 ± 0.014	1.09 ± 0.02	0.927 ± 0.003	–	NEAs
253841 2003 YG118	0.925 ± 0.003	1.962 ± 0.007	1.04 ± 0.01	0.932 ± 0.003	–	NEAs
297418 2000 SP43	0.938 ± 0.002	2.038 ± 0.012	1.10 ± 0.01	0.945 ± 0.002	–	NEAs
326290 Akhenaten	0.930 ± 0.007	1.950 ± 0.045	1.02 ± 0.05	0.937 ± 0.007	–	NEAs
2000 DO1[a]	0.951 ± 0.005	–	–	0.958 ± 0.005	0.045 ± 0.015	NEAs
2001 YE4	0.930 ± 0.002	1.985 ± 0.007	1.06 ± 0.01	0.937 ± 0.002	–	NEAs
u2003 EG[a]	0.906 ± 0.004	–	–	0.913 ± 0.004	0.32 ± 0.05	NEAs
u2003 FT3	0.947 ± 0.005	–	–	0.954 ± 0.005	0.12 ± 0.04	NEAs
2005 WX	0.930 ± 0.013	1.933 ± 0.028	1.00 ± 0.04	0.937 ± 0.013	–	NEAs
2008 BT18	0.919 ± 0.001	1.955 ± 0.006	1.04 ± 0.01	0.926 ± 0.001	–	NEAs
2011 YA	0.925 ± 0.002	1.970 ± 0.005	1.05 ± 0.01	0.932 ± 0.002	–	NEAs
2013 KL6	0.933 ± 0.005	1.943 ± 0.029	1.01 ± 0.03	0.940 ± 0.005	–	NEAs

Notes. Unless otherwise specified, values of BI and BII minima are from Ieva et al. (2015). Other values are from [a]this work, [b]De Sanctis et al. (2011a), or [c]De Sanctis et al. (2011b); unless otherwise specified, BI slopes are from the current work. Other values are from [d]Moskovitz et al. (2010).

In Fig. 2 (right-hand panel), we plot Band separation versus BII minimum. A linear trend is clearly visible, in accordance to what seen by Cloutis et al. (1990), Duffard et al. (2004), and De Sanctis et al. (2011a). None of the V-type classes show the tendency to regroup in a specific range of BII minimum values although slight differences can be observed among different classes: Vestoids show the largest range of values; there are no IOs nor fugitives with $BII_{min} > 2$ μm, and NEAs show a small shift towards higher BII minimum values (in agreement with Fig. 2; left-hand panel).

To better interpret the results of our spectral analysis on the various V-type subclasses considered in this study, we plot the statistical distribution of BI and BII centres (Fig. 3) and Band separations and BI slopes (Fig. 4). Because of the inadequately small number of MOVs objects, we will not include this subclass in the following

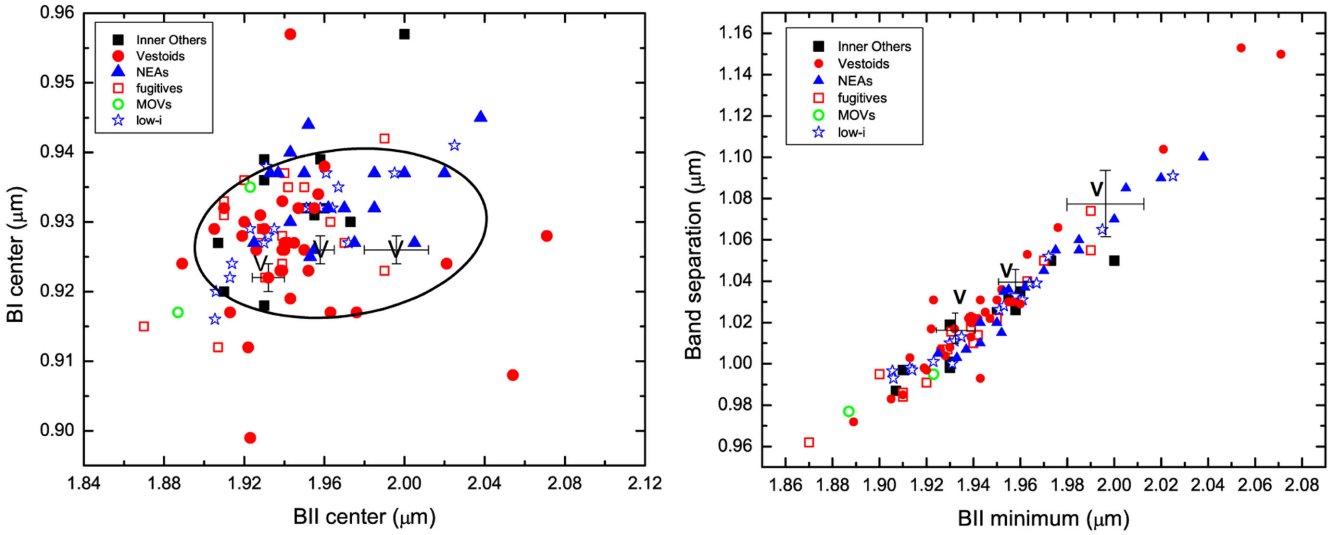

Figure 2. Left-hand panel: BI centre versus BII centre for the different dynamical classes and subclasses of V-types considered in this work: IOs, Vestoids, NEAs, fugitives, MOVs, and low-i (see the main text for details). The V symbols indicate Vesta ground-based observations from Vernazza et al. (2005) while the oval area delimits the range of values obtained by the Dawn spacecraft (De Sanctis et al. 2012). Right-hand panel: Band separation versus BII minimum for the same V-type classes and subclasses considered in the left-hand panel.

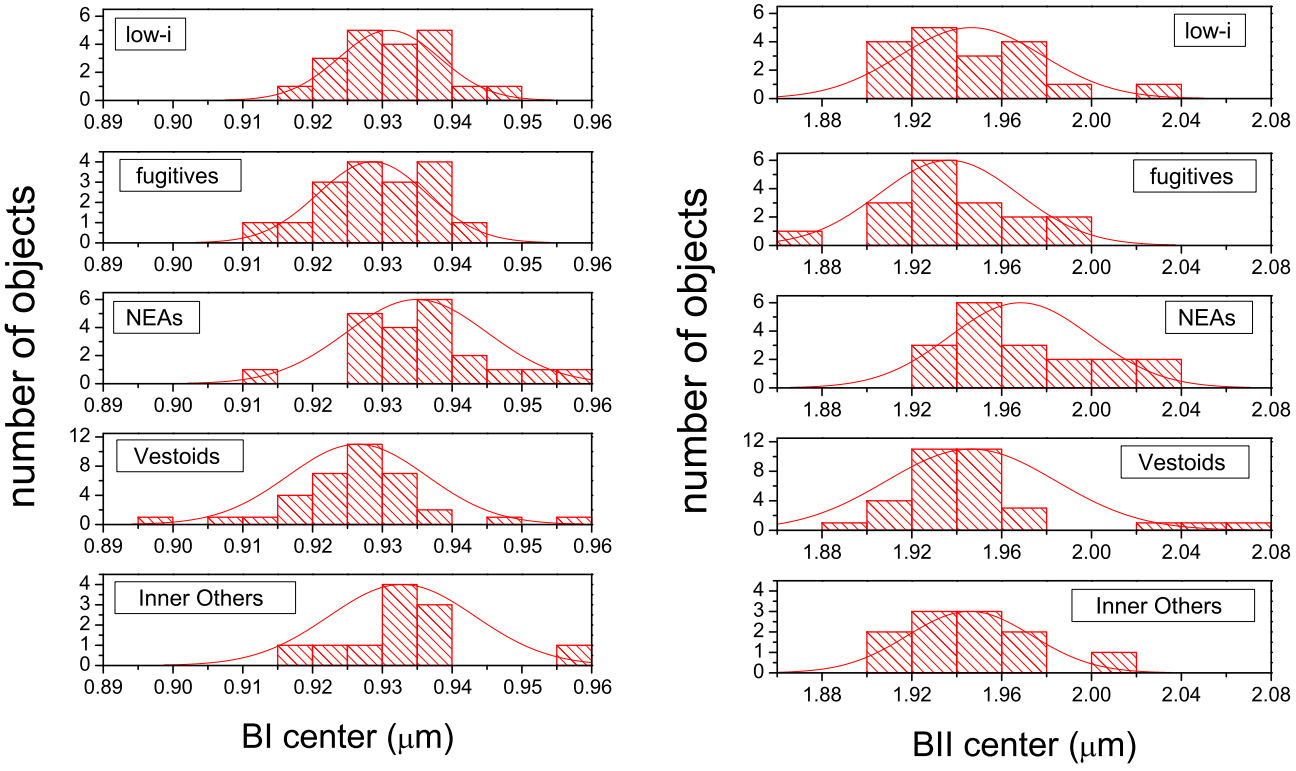

Figure 3. Distribution of BI and BII centres for different V-type subclasses. Note that the curves shown in the graphs are the normal distribution with the same mean and standard deviation of the corresponding set of data (see Table 4).

discussion. Note that the curves shown in the graphs are the normal distribution with the same mean and standard deviation of the corresponding set of data. Mean and standard deviation for each distribution for all V-type subclasses are reported in Table 4. From Fig. 3, it is clear that there are only small differences in the BI centres distributions among the various V-type subclasses, with the only exception for the NEA V-types which show a small shift towards higher BI centre values (the BI centres distribution of the IOs subclass lies mid-way between the one shown by the NEAs and the other V-type subclasses). The same is also true for the BII centres distributions, again with the only exception for the class of NEAs. The Band separation distributions shown in Fig. 4 confirm this general trend (only small differences) among the various V-type subclasses while net discrepancies can be seen when considering the

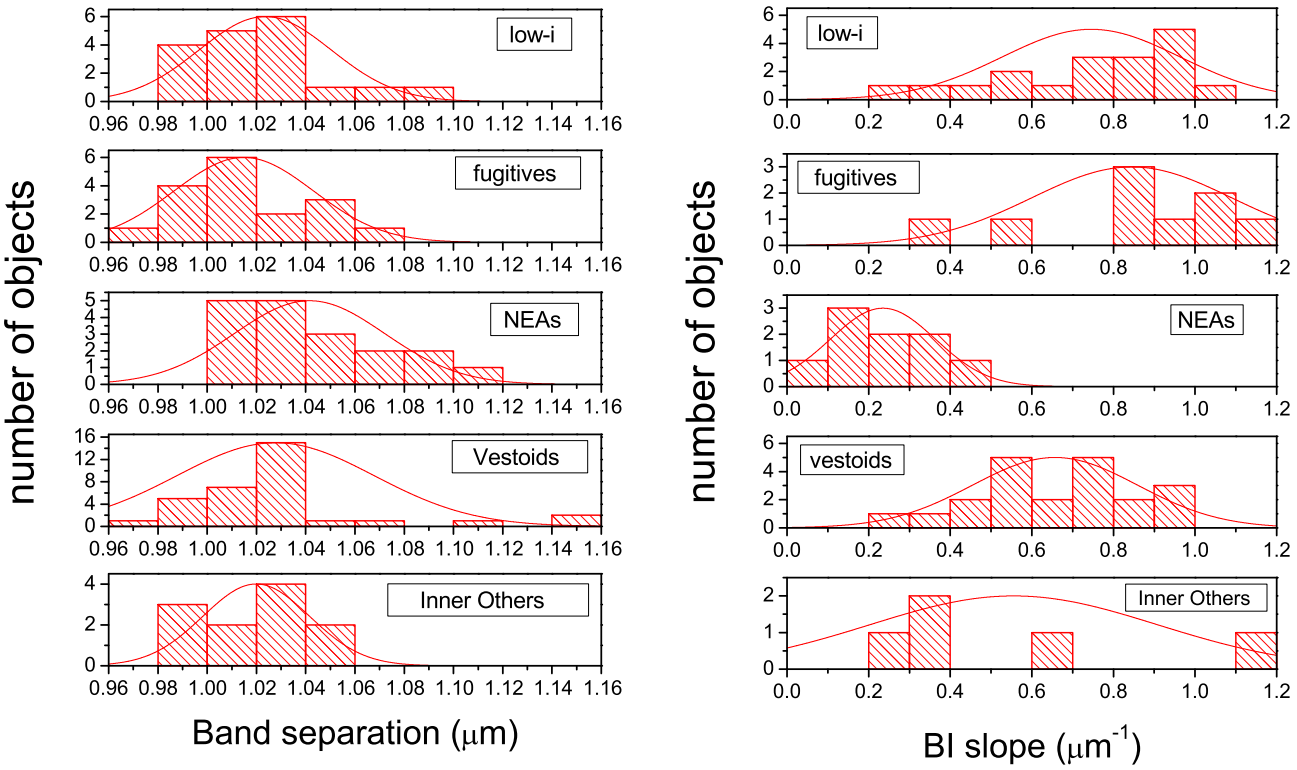

Figure 4. Distribution of Band separations and BI slopes for different V-type subclasses. Note that the curves shown in the graphs are the normal distribution with the same mean and standard deviation of the corresponding set of data (see Table 4).

Table 4. Mean and standard deviation SD (in parenthesis) for the distribution of asteroids belonging to each V-type subclass (curves in Figs 3 and 4).

V-type subclass	BI centre (SD) (μm)	BII centre (SD) (μm)	Band separation (SD) (μm)	BI slope (SD) (μm^{-1})
Low-i	0.931 (0.007)	1.946 (0.032)	1.02 (0.03)	0.75 (0.22)
Fugitives	0.929 (0.008)	1.936 (0.031)	1.01 (0.03)	0.84 (0.24)
NEAs	0.935 (0.01)	1.968 (0.032)	1.04 (0.03)	0.23 (0.13)
Vestoids	0.926 (0.01)	1.946 (0.038)	1.03 (0.04)	0.66 (0.20)
IOs	0.933 (0.01)	1.946 (0.028)	1.02 (0.02)	0.56 (0.35)

BI slopes distributions: first, the class of NEAs shows a BI slopes distribution strongly different from the other V-type subclasses and second, the IOs and Vestoids distributions suggest potential differences when compared to the low-i and fugitives distributions. We want to point out that when considering the results and the data here presented, one should keep in mind that these are based on a relatively limited number of available spectra. Our results suggest that additional observational work is strongly required to test our prediction and to shed light on statistically significant diversities among the spectral properties of V-types belonging to different dynamical subclasses.

5 SPACE WEATHERING EFFECTS

5.1 Experiments on HED meteorites

The term 'space weathering' indicates all processes able to alter the surface spectral properties of minor bodies protected neither by atmosphere nor by magnetic field. For most classes of asteroids, space weathering remains poorly understood mainly because of the scarcity of dedicated experiments (Lazzarin et al. 2006; Brunetto 2009; Gaffey 2010; Vernazza et al. 2013), while it has been mainly studied for the Moon and S-type asteroids. In these cases, the main effect of space weathering is the production of coatings of nanophase metallic iron (Fe) on the surface. These coatings are produced by redeposition of nanophase Fe sputtered by solar wind and cosmic ions and vapors produced by micrometeoritic impacts, and cause changes of the surface reflectance spectra (for details, the reader is invited to refer to Hapke 2001; Chapman 2004; Bennett, Pirim & Orlando 2013; Domingue et al. 2014; Brunetto et al. 2015). Among the different taxonomic classes, the V-type asteroids (Binzel & Xu 1993; DeMeo et al. 2009) are an interesting class and that is why, in recent years, a number of experiments have been conducted on HEDs, to simulate the effects of space weathering processes on Vesta and V-types' surface.

Hiroi & Pieters (1998, and references therein) discussed microsecond pulsed laser irradiation of the diogenite Johnstown. Irradiation effects included darkening and reddening of the VIS-NIR spectra, and weakening of the BI and BII band. Vernazza et al. (2006) performed ion irradiation experiments on the eucrite meteorite Bereba to simulate weathering by the bombardment of solar wind ions. These authors measured a pronounced spectral reddening

Table 5. Bereba and Dar Al Gani 684 (here referred to as DaG) pellets along with used ions, energy, total fluence, BI centre, BII centre, and BI slope.

Pellet	Ion	Energy (keV)	Tot. fluence (ions cm^{-2})	BI centre (μm)	BII centre (μm)	BI slope (μm^{-1})
DaG 1	Before irr.	–	–	0.95	2.063	0.16
DaG 1	Ar^+	200	8×10^{16}	0.952	2.060	0.26
DaG 2	Before irr.	–	–	0.951	2.054	0.22
DaG 2	Ar^+	60	2.5×10^{17}	0.952	2.053	0.30
Bereba 1	Before irr.	–	–	0.944	2.057	−0.07
Bereba 1 (a)	Ar^+	200	4.35×10^{17}	0.950	2.049	0.11
Bereba 1 (b)	C^+	200	a.b. + 3.5×10^{15}	0.950	2.047	0.2
Bereba 2	Before irr.	–	–	0.957	2.098	−0.17
Bereba 2 (a)	Ar^+	200	5×10^{16}	0.958	2.089	−0.16
Bereba 2 (b)	C^+	200	a.b. + 2.3×10^{16}	0.957	2.089	0.08
DaG 3	Before irr.	–	–	0.948	2.061	0.19
DaG 3 (a)	Ar^+	200	5×10^{16}	0.951	2.062	0.23
DaG 3 (b)	C^+	200	a.b. + 3×10^{15}	0.955	2.062	0.33
DaG 3 (c)	Ar^+	200	a.b. + 2×10^{16}	0.955	2.062	0.36
DaG 3 (d)	C^+	200	a.b. + 8×10^{15}	0.955	2.06	0.55
DaG 3 (e)	C^+	200	1.3×10^{16}	0.954	2.05	0.7

Notes. When considering consecutive irradiation steps with the same ion, the total fluence reached with that ion is reported. When a pellet was consecutively irradiated with different ions, 'a.b.' (= as before) appears in the row where the irradiation with the new ion is considered. In that case, the fluence following the 'a.b.' label is the one with the new ion (to be added to the previous value).

and darkening after irradiating Bereba with 400 keV Ar^{++}, and consequently suggested that some mechanism (for instance, protection by a magnetic field) could be responsible for efficiently preventing the reddening of Vesta's surface induced by space weathering. In a recent study, Fulvio et al. (2012) have performed ion irradiation experiments on five samples of two eucrite meteorites (Bereba and Dar Al Gani 684) and analysed the spectral changes induced at different stages of ion irradiation by VIS-NIR reflectance spectroscopy (0.4–2.5 μm). Different ions (Ar^+, C^+) and different energies (from 60 to 200 keV) were used to process the samples. These experiments confirmed that the typical effects of ion irradiation on iron-bearing silicates are also seen for eucrite meteorites: spectral darkening, reddening, and subdued absorption bands with progressive irradiation. In addition, Fulvio et al. (2012) experiments showed that the reddening is much faster (∼100 times) in the case of C^+ than Ar^+ ions and suggested that different HEDs can show different reddening behaviour. In particular, the specific characteristics of each eucrite (i.e. its chemical composition, presence of crystals and their structure, and surface roughness and texture) are able to strongly affect the spectral changes induced by space weathering.

Because of the clear influence of space weathering in changing the overall spectral properties of V-types, we take into account the effects of ion irradiation processing of eucrite meteorites in our analysis and conclusions. To this purpose, we consider the experiments discussed in Fulvio et al. (2012) and estimate the changes induced by ion irraditation on BI and BII centres and BI slopes of Bereba and Dar Al Gani 684 (Table 5). Our aim is to find out the role played by space weathering in the quest for statistically significant differences among the spectral properties of V-type asteroids belonging to different dynamical subclasses.

In Fig. 5, top panel, we plot the changes in BI centre values induced by ion irradiation, as a function of the total irradiation fluence (ions cm^{-2}). We can see that BI centre values change little under ion irradiation, showing only small shifting towards higher values as irradiation proceeds. The biggest relative change in BI centre values is equal to ∽0.007 μm, very small when compared to the range of BI centre values covered by each V-type subclass (Fig. 2). Also, little change is observed for the BII centre values (Fig. 5, middle panel), although in this case BII centre value shift towards lower values as irradiation proceeds. The biggest relative change in BII centre values is equal to about −0.01 μm, like in the previous case very small when compared to the range of values covered by the V-type subclass (Fig. 2). However, stronger variations are seen when considering BI slope values (Fig. 5, bottom panel). In our experiments, the maximum BI slope variation induced by ion irradiation is equal to ∽0.51 μm^{-1}. In this case, the change in BI slope values is appreciable when compared to the range of BI slope values covered by the V-type subclasses (Fig. 6). As irradiation proceeds, the BI slope of eucrite meteorites quickly increases, changing the overall aspect of their VIS-NIR spectra. The shaded area in Fig. 6 shows the region of BI centre values and BI slopes for the eucrites Bereba and Dar Al Gani 684 considered in this work plus a number of eucrites samples from the RELAB data base (www.planetary.brown.edu/relabdata/). Differences between band centre values of eucrites and V-types are discussed in Ieva et al. 2015. Here it is worth noting that the range of BI slope values for the unirradiated Bereba and Dar Al Gani pellets is about −0.17 to 0.22 μm^{-1} while for the eucrites samples from the RELAB data base is about 0.1 to 0.4 μm^{-1}. Besides the limited number of available samples under comparison, this is likely due to the sample preparation: compacted pellets obtained by pressing the original meteorite powder for Bereba and Dar Al Gani pellets in this work (see Fulvio et al. 2012) versus meteorite powder for the RELAB data. A similar difference has been already observed for CC meteorites, in which case the sample preparation (powder versus pressed pellet) does not seem to affect the absolute degree of reddening induced by ion irradiation (Lazzarin et al. 2006).

We want to point out that the presented changes in BI and BII centre and BI slope as a function of the ion irradiation fluence should be considered for their overall indications and qualitative information rather than for the specific values here derived for Bereba and Dar Al Gani 684. Different eucrite samples show specific responses to ion irradiation and only a more extensive laboratory study on a larger set of meteorites can help, in the future, to have a deeper comprehension of the space weathering effects on eucrites. Things

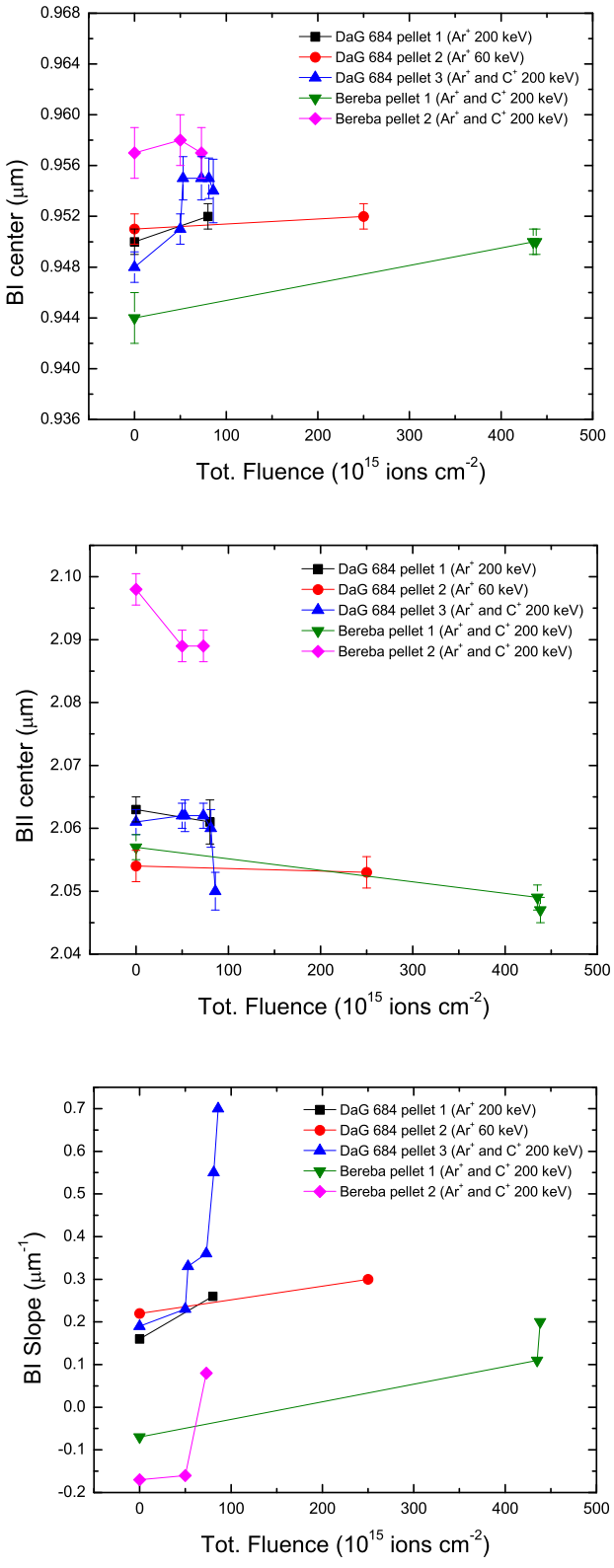

Figure 5. Results of the ion irradiation experiments on the eucrite meteorites Bereba and Dar Al Gani 684 (labelled as DaG 684). Top panel: BI centre versus total irradiation fluence. Middle panel: BII centre versus total irradiation fluence. Bottom panel: BI slope versus total irradiation fluence.

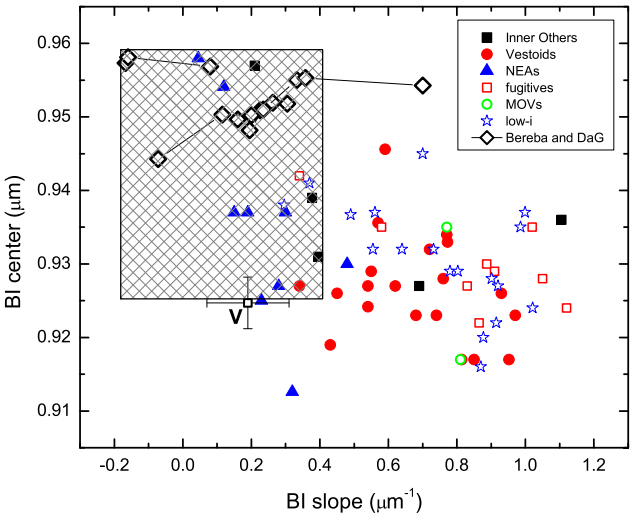

Figure 6. BI centre versus BI slope for the different dynamical subclasses of V-types considered in this work. Changes induced by ion irradiation are also shown (connected diamonds) for the eucrite meteorite Bereba and Dar Al Gani 684. The shaded area shows the region of BI centre values and BI slopes for the eucrites Bereba and Dar Al Gani 684 considered in this work plus a number of eucrites samples from the RELAB data base (see the main text for details). The V symbol indicates BI centre versus BI slope for asteroid Vesta (the value of BI centre is the average from ground-based observations by Vernazza et al. 2005; the value of BI slope is from Vernazza et al. 2006).

are even more complicated when trying to get the 'big picture' on HEDs. One should keep in mind that there are two additional groups of meteorites among the HEDs (Howardites and Diogenites) that so far, to the best of our knowledge, have never been considered for ion irradiation experiments to simulate space weathering effects. Therefore, despite the overall results of our ion irradiation experiments are doubtless valuable, they should be seen as a starting point and additional experimental work is required. Further details of the experimental apparatus and procedures can be found in Brunetto & Strazzulla (2005), and Fulvio et al. (2010, 2012).

5.2 Comparison with the V-types

To better understand the connection between V-type asteroids, Vesta, and HED meteorites, we have compared laboratory spectra of DaG 684 and Bereba before and after different stages of Ar^+ and C^+ irradiation with those of V-types. The comparison has been done for all V-type subclasses considered in this paper. For each subclass, sample spectra of V-types covering the whole range of observed spectral slopes have been taken from SMASS and SMASSIR (http://smass.mit.edu), S3OS2 (Lazzaro et al. 2004), and other studies (Duffard et al. 2004; Alvarez-Candal et al. 2006; Roig et al. 2008; Burbine et al. 2009; Moskovitz et al. 2010; De Sanctis et al. 2011a,b). We note that the energy values used in the ion irradiation experiments discussed in this work are higher than that of 1 keV u^{-1} solar wind C (12 keV) and Ar (36 keV) ions. Therefore, we need to scale the results obtained in the laboratory to evaluate the timescales needed to obtain the same effects in space. The astrophysical time-scale for the solar wind ions to induce the observed spectral changes on an asteroid surface at 2.36 au (average heliocentric distance of asteroid Vesta) has been estimated following the procedure described in Vernazza et al. (2006) and Fulvio et al. (2012). As a reference, laboratory fluence of 10^{15} 200 keV Ar ions cm^{-2}

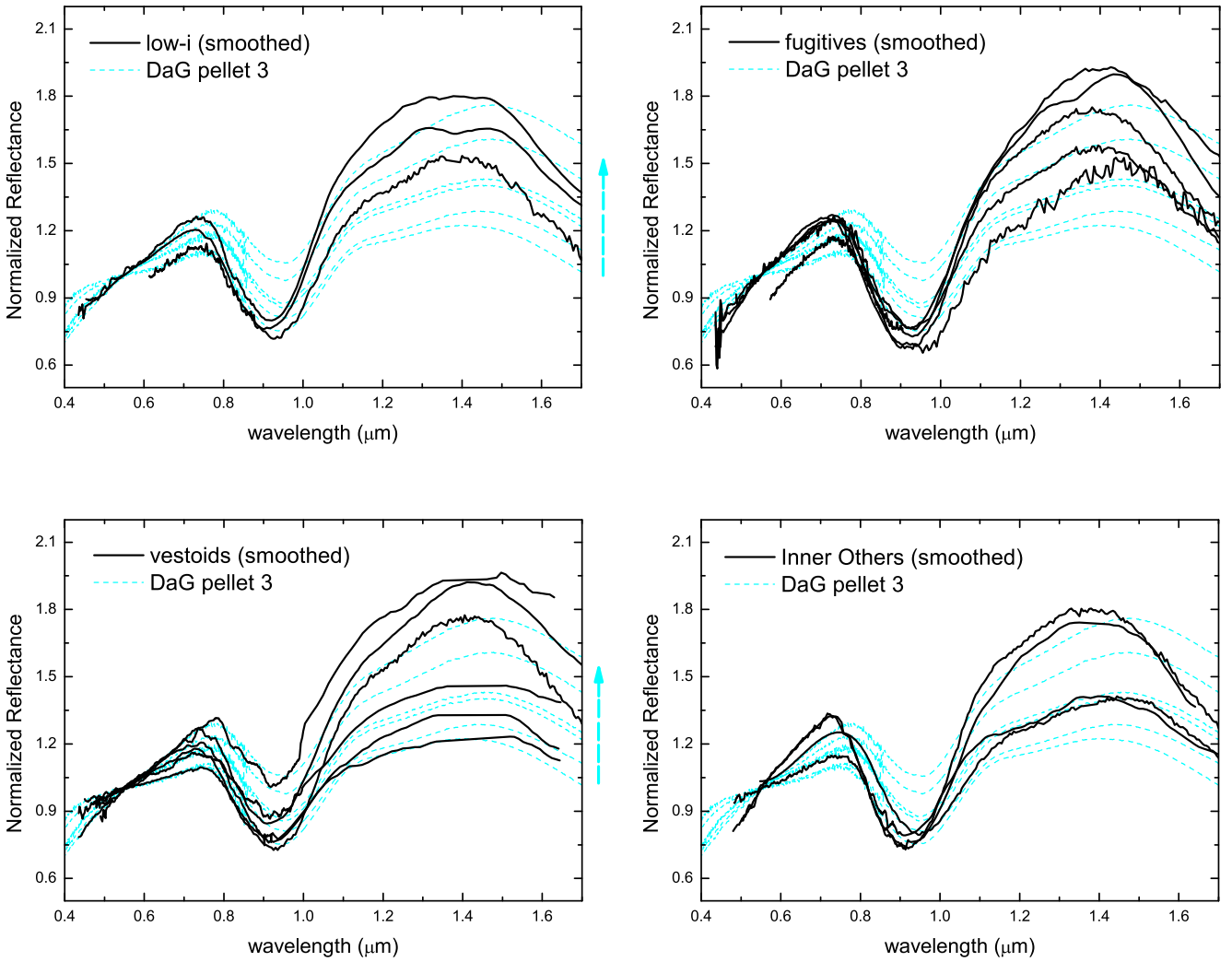

Figure 7. Comparison between VIS-NIR spectra of V-types with spectra of DaG 684 pellet 3 at different stages of ion irradiation. All V-type subclasses discussed in this work are considered, except the one of NEAs (see Fig. 8). Meteorite spectra refer to the irradiation stages reported in Table 5, with increasing irradiation fluence as indicated by the side arrow.

corresponds to about 7×10^3 yr and laboratory fluence of 10^{15} C ions cm^{-2} corresponds to about 1.4×10^4 yr. From Fig. 7, it is clear that for all V-type subclasses (except the one of NEAs, considered in Fig. 8), at the fluences reached in our experiments the weathering effects induced by the ion irradiation experiments are able to cover almost the whole range of BI slopes within a space weathering time-scale $\sim 7.5 \times 10^5$ yr (corresponding to the final fluence reached for DaG 684 pellet 3, taking into account both C and Ar ions irradiation steps). On the other hand, for the V-type NEAs (Fig. 8), experiments show that the weathering effects should cause NEAs' reflectance spectra to be much redder than they actually appear. Although there are experimental limitations that do not allow us to easily simulate space weathering time-scales longer than 10^6–10^7 yr, our results clearly indicate that these time-scales are long enough for V-type asteroids to experience strong reddening able to alter their surface and reproduce the whole range of observed spectral slopes, with no significant differences among V-types subclasses. Special reference needs to be made to the case of V-type NEAs. In the view of the ion irradiation results and the BI slope distributions discussed in this study for the various V-type subclasses, it seems puzzling that V-type NEAs show less-weathered spectra: NEAs' reflectance spectra

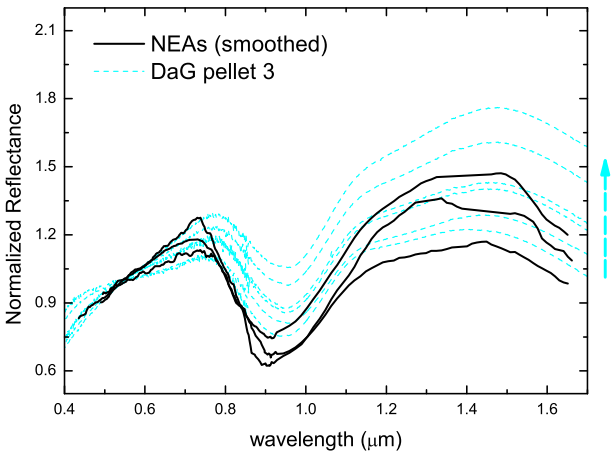

Figure 8. Comparison between VIS-NIR spectra of V-type NEAs with spectra of DaG 684 pellet 3 at different stages of ion irradiation. Meteorite spectra refer to the irradiation stages reported in Table 5, with increasing irradiation fluence as indicated by the side arrow.

should be much redder than they actually appear, in accordance to all other subclasses and possibly even more weathered. This would be due to the fact that the solar wind flux at NEAs' location is higher than for asteroids in the main belt as it decreases with the square of the distance from the Sun. Implications of our results will be discussed in the next section.

6 ASTROPHYSICAL IMPLICATIONS AND CONCLUSIONS

We have reported new NIR (0.8–2.4 μm) spectroscopic observations of seven non-Vestoids, using the NICS instrument at the TNG-INAF (La Palma, Spain). After grouping the totality of V-type asteroids with known NIR spectra in six dynamical subclasses (Vestoids, fugitives, IOs, low-i, NEAs, and MOVs), we have performed a detailed analysis on their spectra, to shed light on similarities and differences among different subclasses and, therefore, on their origin and evolution. We estimated BI and BII centres, Band separations, and BI slopes for 102 V-type asteroids. When considering BI and BII centres, all the considered subclasses show comparable distributions of values, the only exception being the NEAs. This subclass shows centre values slightly higher than all the other ones. On the contrary, net discrepancies can be seen when considering the BI slope distributions: first, the class of NEAs shows a distribution strongly different from all the other V-type subclasses and, second, the IOs and Vestoids distributions suggest possible differences when compared to the low-i and fugitives distributions. However, this last point is based on a limited number of available spectra (especially in the case of fugitives and IOs) and additional observational work is needed to clarify it. Observations should also focus on the search for V-types in the middle/outer main belt. To date only few objects have been detected in this region of the Solar system, although their existence could be one of the strongest proofs of basaltic parent bodies other than Vesta.

The uniqueness of the BI slope in the quest for statistically significant spectral diversities among different V-type subclasses is confirmed by the results of ion irradiation experiments on eucrite meteorites. Strong effects are seen on BI slope values. For the maximum fluence reached in our experiments, the maximum BI slope variation induced by ion irradiation is equal to $\backsim$0.51 μm^{-1}. The change in BI slope values is therefore appreciable when compared to the range of BI slope values covered by the V-type subclasses. As irradiation proceeds, the BI slope of eucrite meteorites quickly increases, changing the overall aspect of their VIS-NIR spectra. The same cannot be said for the effects of ion irradiation on BI and BII centre values. In this case, only little effects are observed as a function of ion processing, very small changes compared to the range of BI and BII centre values covered by each V-type subclass.

By comparing laboratory spectra with asteroid spectra, we have shown that time-scales of the order of 10^5–10^7 yr are long enough for V-type asteroids to experience strong reddening. We have also shown that space weathering effects may explain the whole range of spectral slopes observed for all V-type subclasses, except for the NEAs subclass where only moderate space weathering effects are evidenced. In the view of the ion irradiation results discussed in this study, it is puzzling that V-type NEAs show less-weathered spectra: NEAs' reflectance spectra should be much redder than they actually appear, in accordance to all other V-type subclasses.

As a matter of fact, V-types are not the only taxonomic class of NEAs showing surprisingly pristine surfaces. Unweathered surfaces are also shown by Q-type NEAs, which have collisional and dynamical lifetimes larger than typical time-scales for ion processing to modify their surfaces from 'unweathered' (Q-type) to 'weathered' (S-type) spectra (weathering time-scales of the order of 10^5–10^6 yr). In the case of Q-type NEAs, two implications of the balance among time-scales are that (1) their surface must experience some kind of frequent rejuvenative process and (2) collisions cannot be the main mechanism responsible for the existence of unweathered Q-type NEAs. Close encounters of NEAs with the terrestrial planets have been proposed as the responsible process (see for instance Nesvorný et al. 2005, 2010; Marchi et al. 2006; Vernazza et al. 2009) for producing tidal perturbations to their surface that may remove or mix up the upper and weathered layers of the asteroid surface, therefore exposing 'fresh' unweathered material from lower surface layers. Binzel et al. (2010) have analysed the spectral and orbital properties of 20 Q-type and 75 S-type NEAs. They have shown that Earth encounters are the most probable origin of the 'fresh' surface of Q-type NEAs, which present Minimum Orbit Intersection Distance (MOID) values smaller than ∼0.17 au, with a median MOID value of ∼0.05 au. Conversely, the (weathered) S-type NEAs show a broader distribution with respect to this parameter, up to MOID values larger than ∼0.7 au, and a median MOID of ∼0.1 au. We stress that while the MOID does not give information on specific encounter events, its value can be used to evaluate how close Earth encounters can be, hence how efficient the resurfacing can be. Noteworthy, 18 out of the 21 V-type NEAs in our sample present an MOID $<$ 0.17 au, with the only exceptions of 2000 XH44 (0.23 au), Magellan (0.24 au), and 2003 EG (0.36 au). The median MOID value we find for V-type NEAs is of just 0.035 au, even smaller than the median MOID value for the Q-type NEAs analysed by Binzel et al. (2010). Hence, we propose that the less-weathered surfaces clearly shown by V-type NEAs may be due to close orbital intersections among these asteroids andthe Earth, similarly to what experienced by Q-type NEAs. Such finding also implies that V-type NEAs should deserve a special attention in terms of impact risk analysis (e.g. Perna, Barucci & Fulchignoni 2013). Our results strongly support the need for further observational and theoretical work to investigate in detail the orbital evolution, collisional properties, and consequences of planetary encounters experienced by V-type NEAs.

ACKNOWLEDGEMENTS

Observations have been carried out with the Italian TNG operated on the island of La Palma by the Fundacion Galileo Galilei of the INAF at the Spanish Observatorio del Roque de los Muchachos of the Instituto de Astrofisica de Canarias (programmes AOT19/DDT4 and AOT20/TAC4). We thank Alvaro Alvarez-Candal, who kindly made the data published in his paper available to us. The research of ZK has been supported by VEGA – The Slovak Agency for Science, Grant No. 2/0032/14. DP and SI acknowledge financial support from the NEOShield-2 project, funded by the European Commission's Horizon 2020 programme (Contract No. PROTEC-2-2014-640351).

REFERENCES

Alvarez-Candal A., Duffard R., Lazzaro D., Michtchenko T., 2006, A&A, 459, 969
Bennett C. J., Pirim C., Orlando T. M., 2013, Chem. Rev., 113, 9086
Binzel R. P., Xu S., 1993, Science, 260, 186
Binzel R. P., Gaffey M. J., Thomas P. C., Zellner B. H., Storrs A. D., Wells E. N., 1997, Icarus, 128, 95

Binzel R. P., Rivkin A. S., Stuart J. S., Harris A. W., Bus S. J., Burbine T. H., 2004, Icarus, 170, 259
Binzel R. P. et al., 2010, Nature, 463, 331
Brunetto R., 2009, Earth Moon Planets, 105, 249
Brunetto R., Strazzulla G., 2005, Icarus, 179, 265
Brunetto R., Loeffler M. J., Nesvorný D., Sasaki S., Strazzulla G., 2015, in Michel P., DeMeo F. E., Bottke W. F., Jr, eds, Asteroids IV. Univ. Arizona Press, Tucson, AZ
Burbine T. H., Buchanan P. C., Dolkar T., Binzel R. P., 2009, Meteorit. Planet. Sci. 44, 1331
Carruba V., Michtchenko T. A., Roig F., Ferraz-Mello S., Nesvorný D., 2005, A&A, 441, 819
Chapman C. R., 2004, Annu. Rev. Earth Planet. Sci., 32, 539
Cloutis E. A., Gaffey M. J., 1991, J. Geophys. Res., 96, 22809
Cloutis E. A., Gaffey M. J., Smith D. G. W., Lambert R. S. J., 1990, J. Geophys. Res., 95, 8323
De Sanctis M. C., Ammannito E., Migliorini A., Lazzaro D., Capria Maria T., McFadden L., 2011a, MNRAS, 412, 2318
De Sanctis M. C., Migliorini A., Luzia Jasmin F., Lazzaro D., Filacchione G., Marchi S., Ammannito E., Capria M. T., 2011b, A&A, 533, A77
De Sanctis M. C. et al., 2012, Science, 336, 697
DeMeo F. E., Binzel R. P., Slivan S. M., Bus S. J., 2009, Icarus, 202, 160
Domingue D. L. et al., 2014, Space Sci. Rev., 181, 121
Duffard R., Lazzaro D., Licandro J., De Sanctis M. C., Capria M. T., Carvano J. M., 2004, Icarus, 171, 120
Fulvio D., Guglielmino S., Favone T., Palumbo M. E., 2010, A&A, 511, 62
Fulvio D., Brunetto R., Vernazza P., Strazzulla G., 2012, A&A, 537, L11
Gaffey M. J., 1997, Icarus, 127, 130
Gaffey M. J., 2010, Icarus, 209, 564
Gaffey M. J., Cloutis E. A., Kelley M. S., Reed K. L., 2002, in Bottke W. F., Jr, Cellino A., Paolicchi P., Binzel R. P., eds, Asteroid III. Univ. Arizona Press, Tucson, NZ, p. 183
Hapke B., 2001, J. Geophys. Res., 106, 10039
Hiroi T., Pieters C. M., 1998, Antarct. Meteorit. Res., 11, 163
Hiroi T., Sasaki S., 2001, Meteorit. Planet. Sci., 36, 1587
Ieva S. et al., 2014, A&A, 569, A59
Ieva S. et al., 2015, MNRAS, in press
Jaumann R. et al., 2012, Science, 336, 687
Klima R. L., Pieters C. M., Dyar M. D., 2007, Meteorit. Planet. Sci., 42, 235
Lazzarin M., Marchi S., Moroz L. V., Brunetto R., Magrin S., Paolicchi P., Strazzulla G., 2006, ApJ, 647, L179
Lazzaro D. et al., 2000, Science, 288, 2033
Lazzaro D., Angeli C. A., Carvano T., Mothe-Diniz J. M., Duffard R., Florczak M., 2004, Icarus, 172, 179
McCord T. B., Adams J. B., Johnson T. V., 1970, Science, 168, 1445
McFadden L. A., McCord T. B., Pieters C., 1977, Icarus, 31, 439
Marchi S., Magrin S., Nesvorný D., Paolicchi P., Lazzarin M., 2006, MNRAS, 368, L39
Marchi S. et al., 2012, Science, 336, 690
Migliorini F., Morbidelli A., Zappala V., Gladman B. J., Bailey M. E., Cellino A., 1997, Meteorit. Planet. Sci., 32, 903
Moskovitz N. A., Willman M., Burbine T. H., Binzel R. P., Bus S. J., 2010, Icarus, 208, 773
Nesvorný D., 2012, Nesvorny HCM Asteroid Families V2.0. EAR-A-VARGBDET-5-NESVORNYFAM-V2.0. NASA Planetary Data System
Nesvorný D., Jedicke R., Whiteley R. J., Ivezić Z., 2005, Icarus, 173, 132
Nesvorný D., Roig F., Gladman B., Lazzaro D., Carruba V., Mothé-Diniz T., 2008, Icarus, 193, 85
Nesvorný D., Bottke W. F., Vokrouhlický D., Chapman C. R., Rafkin S., 2010, Icarus, 209, 510
Perna D. et al., 2010, A&A, 513, L4
Perna D., Barucci M. A., Fulchignoni M., 2013, A&AR, 21, 65
Roig F., Nesvorný D., Gil-Hutton R., Lazzaro D., 2008, Icarus, 194, 125
Russell C. T. et al., 2012, Science, 336, 684
Scott E. R. D., Greenwood R. C., Franchi I. A., Sanders I. S., 2009, Geochim. Cosmochim. Acta, 73, 5835
Strazzulla G., Dotto E., Binzel R., Brunetto R., Barucci M. A., Blanco A., Orofino V., 2005, Icarus, 174, 31
Thomas P. C., Binzel R. P., Gaffey M. J., Storrs A. D., Wells E. N., Zellner B. H., 1997, Science, 277, 1492
Vernazza P., Mothé-Diniz T., Barucci M. A., Birlan M., Carvano J. M., Strazzulla G., Fulchignoni M., Migliorini A., 2005, A&A, 436, 1113
Vernazza P., Brunetto R., Strazzulla G., Fulchignoni M., Rochette P., Meyer-Vernet N., Zouganelis I., 2006, A&A, 451, L43
Vernazza P., Binzel R. P., Rossi A., Fulchignoni M., Birlan M., 2009, Nature, 458, 993
Vernazza P. et al., 2013, Icarus, 225, 517
Zappala V., Bendjoya Ph., Cellino A., Farinella P., Froeschlé C., 1995, Icarus, 116, 291

This paper has been typeset from a TEX/LATEX file prepared by the author.